Heliyon 8 (2022) e11598

Contents lists available at ScienceDirect

Heliyon

journal homepage: www.cell.com/heliyon

Research article

Phase change material infused recycled brick aggregate in 3D printed concrete

Heidi Christen [a,*], Seung Cho [a,b], Gideon van Zijl [a], Wibke de Villiers [a]

[a] Stellenbosch University, Private Bag X1, Matieland, 7600, Stellenbosch, South Africa
[b] Ulsan National Institute of Science and Technology (UNIST), 44919, Ulsan, Republic of Korea

HIGHLIGHTS

- Thermal energy storage recycled brick aggregates are created by vacuum impregnation.
- 3D printable thermal energy storage concrete is created and termed PCM-3DPC.
- PCM-3DPC has higher buildability than 3D printed concrete.
- PCM-3DPC compressive and tensile strengths are comparable to 3D printed concrete.
- No negative effects of phase change material on 90-day compressive cube strength.

ARTICLE INFO

Keywords:
3D printed concrete
Additive manufacturing
Phase change material
Recycled brick aggregate
Rheological and mechanical characterization

ABSTRACT

In this paper the effects of the addition of a paraffin phase change material on the strength and printability of 3D printed concrete are studied. Phase change materials are latent heat storing materials, which garner and release large amounts of energy as they change phase. The addition of phase change materials to concrete produces a composite material with maximised latent and sensible heat storage capacity. Used in buildings, this composite material has the ability to minimise unwanted heat transfer across the building envelope.

An existing mix design (RBA-3DPC), in which 64% of the natural aggregate in a 3D printable concrete (3DPC) had been replaced with recycled brick aggregate, is adjusted by adding phase change material to the pores of the recycled brick aggregate by vacuum impregnation, creating PCM-3DPC. Rheological characterisation tests are performed on reference mix designs (3DPC and RBA-3DPC) and the PCM-3DPC mix design, and used in a buildability model to validate the number of printable layers. Mechanical characterisation tests including cube strength tests, direct tensile tests and uniaxial compressive tests are performed on cast and printed specimens of the mix designs. There is no existing research on the effects of the combined addition of recycled brick aggregate and phase change material in 3D printed concrete.

It is concluded that the PCM-3DPC has the highest number of printable layers predicted by the model and realised by a cylindrical column print and overall, PCM-3DPC has greater strength compared to RBA-3DPC, and lower strength compared to 3DPC. The PCM-3DPC exceeds the RBA-3DPC interlayer tensile strength by 6%, intralayer compressive strength by 43% and interlayer compressive strength by 9%, and subceeds the 3DPC interlayer tensile strength by 15% and interlayer compressive strength by 13%.

1. Introduction

There are three main phases of the building sector which should be considered in the effort to improve its sustainability, and these are the construction phase, the operation phase and the demolition phase. In research by Christen et al. [1], the recycling and automation potential in the construction and demolition phases were realised by the incorporation of recycled brick aggregate (RBA) in 3D printed concrete (3DPC) to create RBA-3DPC.

Apart from the energy and resources required during the construction phase of a building, large amounts of energy are required in its operation phase, to maintain comfortability inside the building. According to the

* Corresponding author.
E-mail address: 19189109@sun.ac.za (H. Christen).

https://doi.org/10.1016/j.heliyon.2022.e11598
Received 11 August 2022; Received in revised form 11 October 2022; Accepted 9 November 2022

latest synthesis report from the Intergovernmental Panel on Climate Change [2], the building sector is the third largest contributor to greenhouse gas emissions. The direct greenhouse gas emissions of the building sector are relatively low, but when indirect CO_2 emissions of electricity and heat production are taken into account, the share of emissions from the building sector increases from 6.4% to 18.4%.

To provide a thermally comfortable environment inside buildings, air-conditioning systems are typically used, which require vast amounts of energy, and therefore indirectly add to the problem of climate change. As temperatures rise across the globe, the temperature difference that needs to be maintained across the building envelope also increases. Instead of relying solely on air-conditioning systems to provide this temperature difference and maintain thermal comfort inside buildings, passive design solutions can be applied to create a building envelope with more efficient thermal insulation properties, so that the transfer of unwanted heat across the building envelope is minimised [3]. Phase change materials (PCMs) are one such passive design solution, which have thermal energy storage potential due to their high latent heat capacity.

The objective of this research paper is to assess the combined effect of PCM and RBA on the rheological and mechanical properties of a 3DPC mix. RBA is a variable material, with high porosity and water absorption. RBA is therefore expected to affect the rheological performance of a 3DPC mix by altering its viscosity and yield stress, and is known to negatively affect the strength of a 3DPC mix [1]. It is so far unknown how the addition of PCM to the pores of the RBA will change the rheological and mechanical properties of the 3DPC.

A latent heat storing PCM is incorporated into the RBA-3DPC mix design, thus developing what will be referred to as PCM-3DPC. The thermal efficiency of PCM inside concrete specimens has already been proven by Cabeza et al. [4], Gassar and Yun [5], Hassan et al. [6] and Mankel et al. [7], among others, but there is currently very little research on the addition of PCM to 3DPC. No research currently exists on PCM inclusion in 3DPC by aggregate impregnation of RBA. As an initiation phase of this attempt, the mix design development and material characterisation are essential prior to investigating actual thermal performance. It is thus worthwhile to mention that this research purposefully focuses on the development and characterisation of the novel material, while validation of the thermal performance of PCM-3DPC is carried out separately by the authors. Due to the lack of formwork in additive manufacturing, the rheology of a 3DPC mix design is an important material property to perfect for acceptable pumpability, extrudability, shape retention and buildability. It is also important that 3DPC hardened mechanical properties should not be adversely affected, given known reduced compressive strength by morphologically altered microstructure through extrusion 3D printing, and anisotropy due to lack of fusion between layers.

A PCM was chosen with a phase change temperature and characteristics suitable to the application, and a PCM-3DPC mix design was developed, using the RBA-3DPC mix as a reference. A rheological characterisation was performed on the PCM-3DPC mix, as well as two existing mix designs - 3DPC and RBA-3DPC, recorded by Christen et al. [1] - for comparison. The rheological characterisation was used in a buildability model developed by Kruger et al. [8], which was validated by the print-to-collapse test of the three mixes. Mechanical characterisation tests were carried out on specimens cut from a 3D printed rectangular section of the PCM-3DPC mix and compared to results of 3DPC and RBA-3DPC mechanical characterisation tests [1]. For an understanding of the PCM leakage occurring from the pores of the RBA, scanning electron microscopy (SEM) imaging, 90-day strength tests and mass loss tests were carried out on cast and printed samples of the PCM-3DPC mix design.

2. Phase change material

PCMs are latent heat storing materials, with the ability to accumulate and release thermal heat as they change phase. Used in concrete, PCMs could reduce the energy requirement for heating and cooling building interiors, because of their more efficient thermal properties [9].

PCMs have the ability to store heat as both sensible and latent heat [10]. Energy is stored as sensible heat in a material by causing an increase in the temperature of the material. The relationship between the amount of heat stored and the increase in temperature of the material is determined by the specific heat capacity of the material, and is defined in Eq. (1):

$$Q = mC_{ap}(T_f - T_i) \tag{1}$$

where Q is the amount of heat stored (J), T_i is the initial temperature (°C), T_f is the final temperature (°C), m is the mass of the material storing heat (kg) and C_{ap} is the average specific heat capacity (J/kgK) over the temperature range from T_i to T_f.

Energy is stored as latent heat when heat is absorbed or released during the phase change of a material. This phase change could be solid to solid (when the material changes from one crystalline form to another), solid to liquid, liquid to gas, or the reverse of any of these. Latent heat storage is the most efficient method of thermal energy storage due to its high storage density and the narrow temperature range be-

Table 1. Properties of RT25HC used in study [19].

Melting temperature range (°C)	22–26
Peak melting temperature (°C)	25
Specific heat capacity (kJ/kg °C)	2
Latent heat capacity (kJ/kg)	200
Thermal conductivity (W/m °C)	0.2

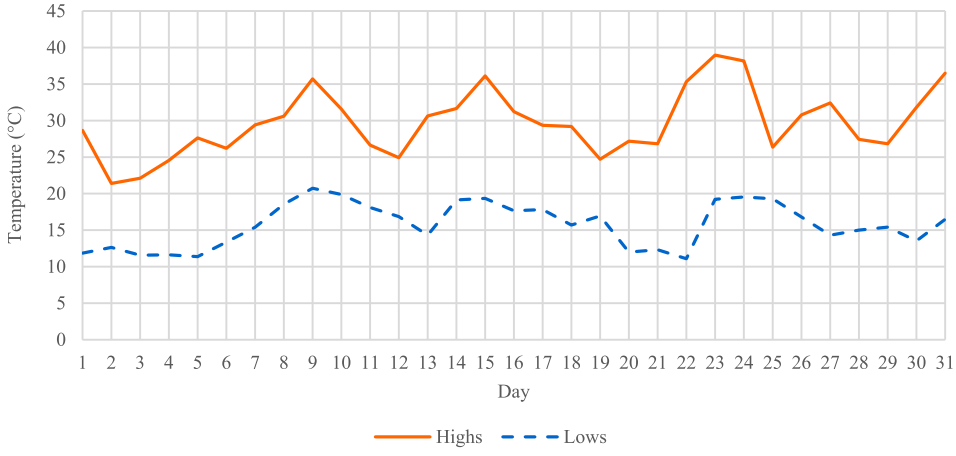

Figure 1. Outdoor ambient temperatures in Stellenbosch in January 2022 [18].

tween the store and release of heat [11]. The heat stored by a phase change system has a sensible and latent heat contribution and is defined in Eq. (2) [12]:

$$Q = \int_{T_i}^{T_m} mC_p dT + ma_m \Delta H_m + \int_{T_m}^{T_f} mC_p dT \quad (2)$$

where T_m is the phase change temperature (°C), C_p is the specific heat capacity as a function of temperature (J/kg°C), a_m is the fraction of the material which has changed phase, and ΔH_m is the heat of phase change per unit mass (J/kg).

2.1. Incorporation of phase change materials in concrete

Concrete is a building material with a high thermal mass [13] related to its high density and high specific heat capacity. Concrete therefore has good sensible heat storage ability, which is one of the reasons for it being the most widely used building material today. Incorporating PCMs inside concrete introduces the potential for thermal storage as latent as well as sensible heat, maximising the total thermal storage capacity [14]. PCM-concrete can be created by 4 typical techniques of incorporating the PCM into the concrete. These techniques are [9]:

- Immersion of porous concretes,
- Aggregate impregnation,
- Direct mixing of micro-encapsulated PCMs into the concrete mix,
- Macro-encapsulation.

In this study, it was intended that the RBA-3DPC mix design would be used and adapted to include PCM in the pores of the recycled brick aggregate. Aggregate impregnation was therefore chosen as the method of incorporation of PCM in concrete. The aggregate impregnation and immersion techniques are similar in that they rely on the porosity and absorptive capacity of a material to carry PCM inside its pores. Unlike the immersion technique, which immerses finished concrete products in PCM, aggregate impregnation relies on two steps:

1. Thermal Energy Storage Aggregates (TESAs) are created by adding a liquid PCM into the pores of aggregates by vacuum impregnation.
2. Thermal Energy Storage Concrete (TESC) is created by mixing TESAs with cement and other concrete mix constituents.

The advantages of the aggregate impregnation technique compared to the immersion technique is that higher levels of PCM can be incorporated with lower chances of leakage and pollution [15]. Zhang et al. [15] confirmed that the capacity for PCM absorption increased as porosity increased, and density decreased.

To further reduce the possibility of leakage of PCM into the concrete, research is being done on coating techniques for the TESAs. Hassan et al. [16] investigated the effects of coating a lightweight expanded clay aggregate (LECA), that had been impregnated with PCM, with geo-polymer paste. This method of coating was found to be effective, without weight loss or obvious surface wetting during up to 1000 thermal cycles of 15–105 °C and 23–65 °C.

Table 2. Fractions of RBA for PCM-3DPC mix [1].

Sieve size (mm)	% mass retained on sieve
2.000–4.750	6.3
1.000–2.000	33.2
0.600–1.000	31.3
0.425–0.600	14.5
0.300–0.425	14.7

Table 3. Summary of data for calculation of PCM absorption.

Solid density of PCM (kg/m^3)	880
Liquid density of PCM (kg/m^3)	770
Average density of PCM (kg/m^3)	825
Density of water (kg/m^3)	1000
Water absorption (%)	18.2
PCM absorption (%)	15.0

Figure 2. Setup of vacuum desiccator for aggregate impregnation.

The research by Hassan et al. [16] included a technique for aggregate impregnation of paraffin-based PCM into LECA. The LECAs were first heated at 100 °C for 8 h to completely dry the pores of the material. The LECAs were then added to a vacuum desiccator between two sieves with mesh sizes smaller than the particle sizes. Melted PCM was poured through a funnel over the sieves containing the LECAs, filling the vacuum desiccator until the LECAs were completely submerged. The vacuum was applied at 0.95 bar for 30 min, shaking the vacuum desiccator every 5 min to achieve stirring. Throughout the process, the temperature of the PCM was maintained well above its melting temperature to avoid solidification of the PCM during impregnation.

2.2. Phase change material selection

PCMs have various applications in the building and industrial sectors, and there are different types of PCMs which have different suitability to these applications. Pielichowska and Pielichowski [11] and Sharma et al.

Table 4. Mix design development.

	3DPC Mix [1]	RBA-3DPC Mix [1]	PCM-3DPC Mix
Cement (kg)	521.00	521.00	521.00
Fly Ash (kg)	161.00	161.00	161.00
Micro Silica Fume (kg)	81.00	81.00	81.00
Fine Aggregate (kg)	1229.37	442.57	442.57
RBA (kg)	–	562.14	499.55
PCM (kg)	–	–	74.93
Extra water added (% by RBA mass)	–	12%	–
Total water (kg)	235.00	302.46	235.00
Superplasticizer (% by binder mass)	1%	1%	1.3%
VMA (% by binder mass)	0.3%	0.3 %	0.3%
Microfibres (% by total volume)	1%	1%	1%
w/c	0.45	0.58	0.45

[12] defined certain criteria for the properties of a chosen PCM. The criteria include a phase change temperature in the operating temperature range, a high latent heat of phase change, a small volume change due to phase change, congruent melting of PCM, absence of supercooling, chemical stability in the long term, a reversible freeze/melt cycle, compatibility with the other construction materials, non-toxic, non-flammable and non-explosive.

When choosing a suitable PCM for this study, it was important to consider the operating temperature of the PCM, as well as the intended method of incorporation of the PCM in the concrete. A comfortable room temperature is generally considered to fall at around 18–24 °C [17]. For a PCM to be effective, it must have a phase change temperature close to the desired room temperature and falling within the range of temperatures that the building is being subjected to. Weather data from the weather station at Stellenbosch University [18] was assessed to determine typical outdoor ambient temperatures in Stellenbosch in summer. January of 2022 was determined as the hottest month of the summer with an average high of 29.7 °C and an average low of 15.7 °C. A graph of the temperature data for January 2022 is shown in Figure 1.

It is likely that the temperatures reached across the building envelope will be higher or lower than the outdoor ambient temperature at any point in time, and that when exposed to large amounts of solar radiation, the walls of a building may reach temperatures significantly higher than the ambient temperatures recorded in Figure 1. It is assumed that on an average summer's day in Stellenbosch, each point across a building envelope will reach a low less than or equal to 15.7 °C and a high greater than or equal to 29.7 °C. The PCM chosen for this study therefore needed to have a melting temperature between 15.7 and 29.7 °C for it to undergo a melt-freeze cycle and effectively save cooling energy on an average summer's day in Stellenbosch. If a melting temperature below 15.7 °C was chosen, the PCM could be in an almost constant liquid state for many days throughout summer, and its energy saving potential by phase change would be squandered. If a melting temperature above 29.7 °C was chosen, the PCM could be in an almost constant solid state for many days throughout summer, again squandering its energy saving potential by phase change.

By considering the average outdoor ambient temperatures experienced during the hottest month of the summer, and taking into account comfortable indoor temperatures, it was decided that a PCM with a phase change of 25 °C would be used in this study. The energy saving potential by phase change would therefore likely be activated almost every day in summer.

Two types of PCMs from Rubitherm Technologies GmbH were considered for the aggregate impregnation technique: an inorganic PCM, SP25E2, and an organic PCM, RT25HC. The SP25E2 PCM contained

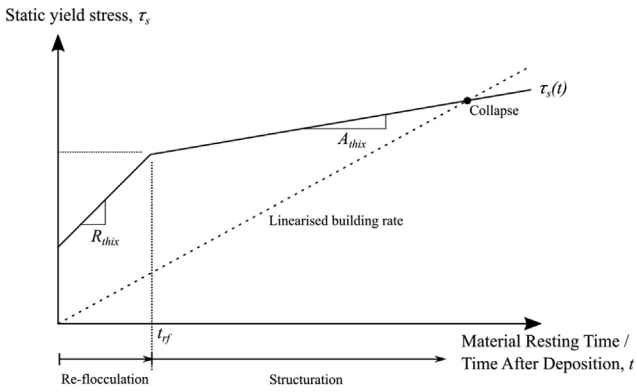

Figure 4. Bi-linear material shear yield stress evolution curve with thixotropic parameters, building rate and predicted failure, re-worked from Kruger et al. [23].

ammonium chloride and when mixed with concrete caused a reaction releasing ammonia into the air. Due to this reaction and the fact that the SP25E2 PCM had a corrosive effect on metals, which would be problematic if any steel reinforcing was used in the 3DPC, it was decided that the SP25E2 would be unsuitable for the application. The organic PCM with a peak melting temperature of 25 °C (RT25HC) was therefore chosen, with the aim of saving cooling energy in the summer months. The properties of this PCM are listed in Table 1.

Organic paraffins are saturated hydrocarbons with a general formula C_nH_{2n+2}. They have a high latent heat capacity, are non-toxic, do not experience phase separation and have a constant thermal performance over thousands of cycles. The melting temperature and heat of fusion of the PCM are generally dependent on the length of the hydrocarbon chain, with longer chains leading to higher melting temperature. Because of this, PCMs can be designed for a specific temperature application by mixing hydrocarbons of different lengths [11].

3. Experimental procedure

3.1. Development of PCM-3DPC

3.1.1. Creation of thermal energy storage aggregates

The reference RBA-3DPC mix design had a 64% replacement of natural aggregate with RBA. The PCM-3DPC mix design was to contain RBA fractions in the same ratios as they were in the RBA-3DPC mix design. The fractions of the RBA in their ratios for the mix designs are shown in Table 2.

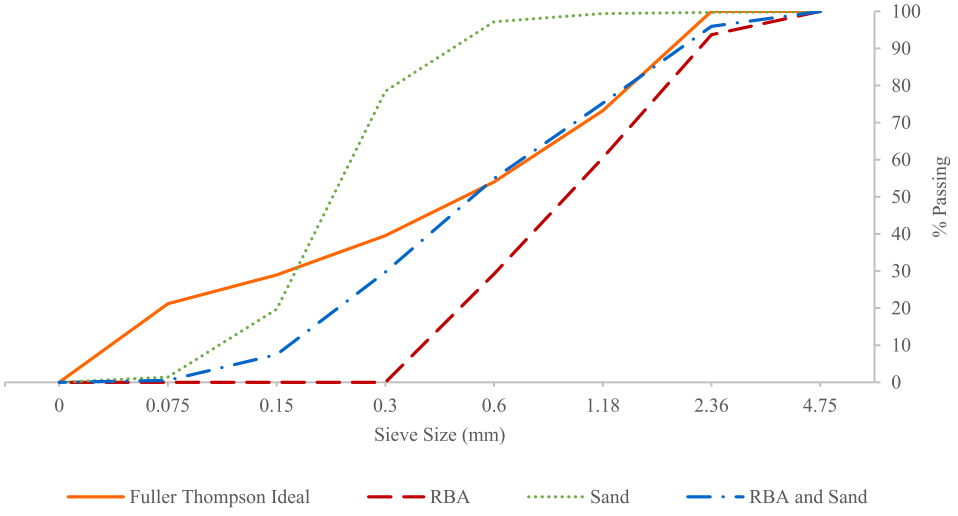

Figure 3. Aggregate grading curves by particle distribution analysis [1].

Due to the increased porosity and water absorption of RBA compared to fine aggregate, extra water was added to the RBA-3DPC mix to achieve acceptable printability. The water absorption (WA) of the RBA had been determined by Christen et al. [1], using SANS3001-AG21 [20], as 18.2%. To adapt the RBA-3DPC mix to incorporate PCM, PCM would be added to the RBA by vacuum impregnation, instead of adding extra water in the mix. This would create thermal energy storage aggregates (TESAs) known as PCM-RBA. To be able to maximise the latent heat capacity of the PCM-3DPC, the upper limit for PCM that could be absorbed in the pores of the RBA was assumed to be equal to the volume of water absorbed during the WA test. The WA is a mass percentage of water absorbed by the RBA to achieve a saturated surface-dry condition. The amount of PCM to be added to the RBA was therefore calculated based on Eq. (3).

$$PCM\ absorption = WA \bullet \rho_{PCM}/\rho_w \tag{3}$$

where ρ_{PCM} is the average of the solid and liquid densities of the PCM (kg/m^3) and ρ_w is the density of water (kg/m^3). The data for the calculation of the PCM absorption is summarised in Table 3.

The setup for the aggregate impregnation technique which involved adding PCM to the pores of RBA by vacuum impregnation is shown in Figure 2. The process involved the following steps:

1. Melt PCM in an oven at 50 °C.
2. Weigh off a batch of RBA with fractions in the ratios listed in Table 2. It was determined that the maximum total mass to be used per batch should be 6 kg, as this would be suitable for the size of the available vacuum desiccator.
3. Pour the weighed off batch of RBA into the desiccator and place in the oven alongside PCM for 1 h.
4. Weigh off the melted PCM (15% by mass of RBA batch).
5. Pour the melted and weighed off PCM into the desiccator containing the RBA. Stir the entire batch to a consistent colour throughout, and place back in the oven to recoup the heat lost while stirring.
6. Remove the desiccator from the oven, attach the lid to the desiccator and apply -0.75 bar vacuum suction to the batch for 1 h. This step should be carried out as quickly as possible so that the vacuum impregnation process can occur while the PCM-RBA is still at high temperature.

3.1.2. Creation of thermal energy storage concrete

The ASTM mini-slump cone test was used to determine acceptable printability of the PCM-3DPC mix, using recommendations by Cho et al. [21], that a flow table diameter reading of 150–165 mm was ideal for acceptable printability, as a guideline. The 3DPC and RBA-3DPC mixes which were used as a reference for the development of the PCM-3DPC mix are shown in Table 4. The first PCM-3DPC mix design that was developed had limited flowability and was deemed unprintable. An adjustment was made by increasing the superplasticiser content of the mix to 1.3% (by binder mass), and PCM-3DPC Mix shown in Table 4 was developed with acceptable printability. The mass percentage of PCM in the PCM-3DPC mix was 3.68% which translated to a latent heat capacity of 7360 J/kg for the PCM-3DPC mix. Assuming a specific heat capacity of 900 J/kg°C for concrete, the interpretation of this value of latent heat capacity is that when reaching a temperature of 25 °C, roughly eight times more energy is required to raise the temperature of the concrete by another degree.

The cement that was used in the mixes was PPC Suretech 52.5 N (CEM II) Portland cement, and the extenders were DuraPozz class F fly ash and micro-silica fume. The fine aggregate was locally sourced sand (grading curve presented in Figure 3), and the additives were polycarboxylate polymer-based superplasticizer, Chryso Premia 310, and hydroxypropyl methyl-cellulose viscosity modifying agent (VMA), Chryso Quad 20. 6-mm polypropylene microfibres with a Young's modulus of 3 GPa, yield stress of 300 MPa and diameter of 30 μm were added for enhanced mechanical capacity. The RBA fractions which are presented in Table 2 and the grading of the RBA and sand combination which was used in both the RBA-3DPC and PCM-3DPC mixes is shown in Figure 3.

3.2. Rheological characterisation and buildability

The rheology and thixotropy were characterised by a rotary concrete rheometer developed by the International Centre for Aggregate Research (ICAR) [22]. The instrument provides two types of tests, namely stress growth test and flow curve test. The former test measures the material resistance response to the constant imposed shear rate, so called controlled shear rate (CSR) test, resulting in a static yield stress (τ_s). The flow curve test applies a series of flow curve points by varying the shear rate to measure the plastic viscosity (μ_p) and dynamic yield stress (τ_d) at zero-strain rate.

Kruger et al. [23] proposed a bi-linear thixotropic model suitable for predicting the fresh behaviour of 3D printable concrete which is modified from a linear thixotropic model by Roussel [24]. Both models are determined by a series of CSRs with various resting time intervals in between the tests. Each CSR was conducted with a constant applied shear rate of 1 s^{-1} which is equivalent to 0.2 revolutions per second to simulate the auger speed of the pump, as elaborated in [23].

The thixotropic parameters, R_{thix} and A_{thix}, can be derived from Eq. (4), presented by Kruger et al. [23]:

$$R_{thix} = \frac{\tau(t) - \tau_{D,i}}{t} \quad for\ t \le t_{rf}$$

$$A_{thix} = \frac{\tau(t) - \tau_{S,i}}{t - t_{rf}} \quad for\ t > t_{rf} \tag{4}$$

where $\tau_{S,i}$ is initial static yield shear stress, $\tau_{D,i}$ is initial dynamic yield shear stress, and t_{rf} is re-flocculation time defined as $t_{rf} = (\tau_{S,i} - \tau_{D,i})/R_{thix}$. The pictorial illustration of the bi-linear model with thixotropic parameters can be found in Figure 4.

The buildability model by Kruger et al. [8] compared the linearised building rate causing gravitational loading to the printed bottom layer by the subsequent layers with the material shear yield stress evolution curve to predict the failure layer in printing (see Figure 4). The detailed calculation for the number of printable layers can be found in the literature. The prediction is compared to the actual 3D printing by a 3-axis gantry 3D printer with a rotor-stator pump at Stellenbosch University [25].

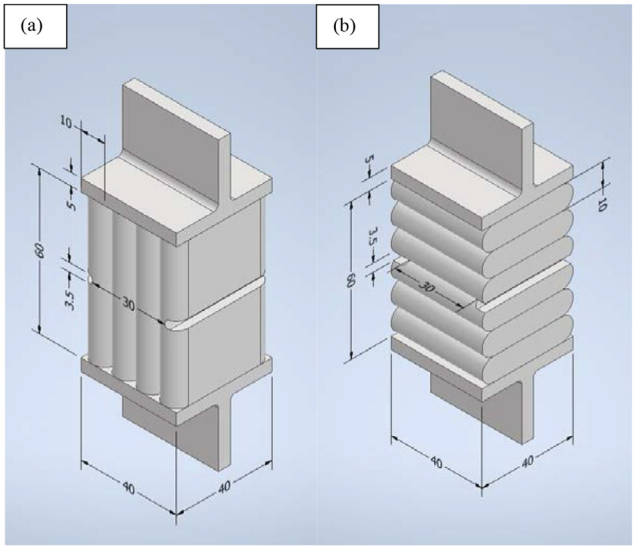

Figure 5. (a) D1 specimen for DTT (b) D3 specimen for DTT [1]. Units in mm.

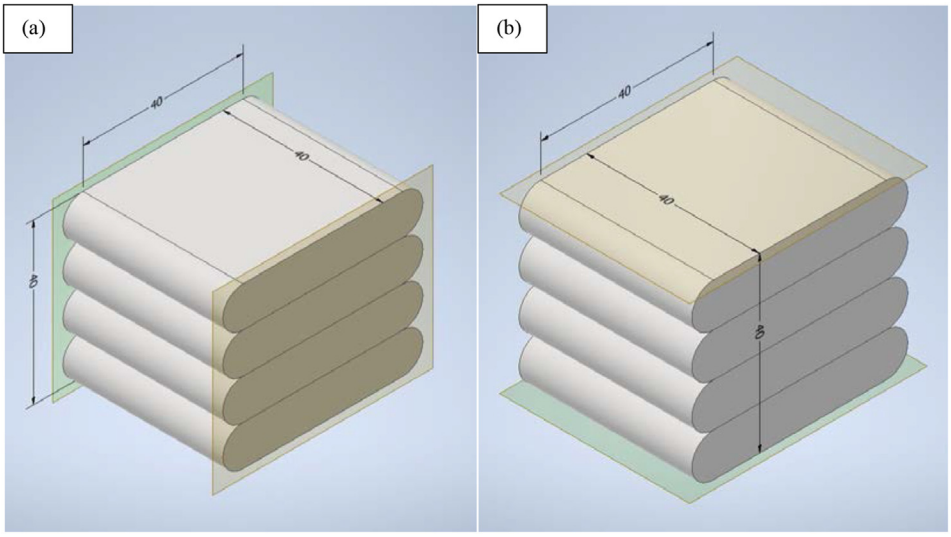

Figure 6. (a) D1 specimen for UCT (b) D3 specimen for UCT [1]. Units in mm.

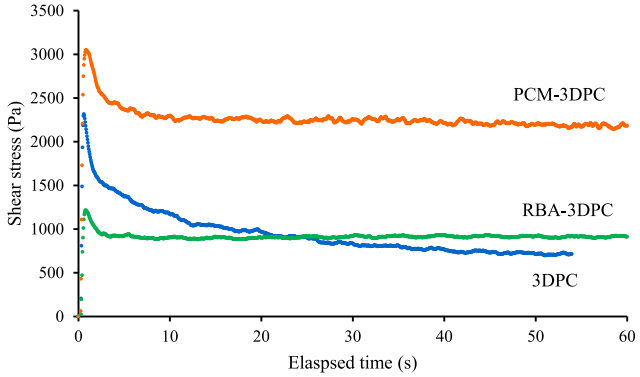

Figure 7. Initial CSR test result for all mixes.

The validation was carried out by printing a 250 mm diameter circular hollow column structure with no infill until failure, so-called print-to-collapse (see Figure 9). Since the model assumes a plastic failure of the material, the buckling effect must be minimised. The circular section is chosen to provide better structural integrity by a constant second moment of area about all axes. A printing speed of 60 mm/s and print path length per layer of 785 mm give a pass time of 13.1 s. The 25 mm diameter circular nozzle produces roughly 40–45 mm filament layer width when a layer height of 10 mm is selected, and a constant flow rate is maintained. To ensure smooth and continuous extrusion, a poker vibrator was placed in the hopper of the pump.

3.3. Mechanical characterisation

Mechanical characterisation tests consisting of 28-day compressive cube strength tests, 28-day tensile 3DPC strength tests and 28-day compressive 3DPC strength tests were performed on the PCM-3DPC mix. The results for the PCM-3DPC mix were compared to the results of the same tests that were performed on the 3DPC and RBA-3DPC mixes.

3.3.1. Compressive cube strength tests

The compressive cube strength tests were performed on cast specimens of the PCM-3DPC mix according to SANS5863 [26]. The cast PCM-3DPC cubes were cured for 28 days in a climate-controlled room with a temperature of 22 ± 2 °C and relative humidity of 65 ± 5%.

3.3.2. Tensile and compressive 3DPC strength tests

Direct tensile tests (DTT) and uniaxial compressive tests (UCT) were performed on specimens cut from a 3D printed section of the PCM-3DPC mix. The section had a path length of 1200 mm and a print speed of 60 mm/s 20 layers were printed with a layer height of 10 mm to give a total height of 200 mm. The PCM-3DPC specimens for the DTTs and UCTs were prepared and tested in the same way as the 3DPC and RBA-3DPC specimens.

For the DTTs, six specimens were cut from the printed section in Direction 1 (D1 – intralayer direction) and six specimens were cut from the printed section in Direction 3 (D3 – interlayer direction). All twelve specimens were notched to ensure a predictable failure plane and then glued with epoxy to steel T-sections, allowing at least 6 days for drying before testing. The D1 and D3 specimens after being notched and glued to

Table 5. Rheological assessment data and buildability result.

	Material properties in fresh-state						
	$\tau_{s,i}$ (Pa)	$\tau_{d,i}$ (Pa)	μ_p (Pa.s)	t_{rf} (s)	R_{thix} (Pa/s)	A_{thix} (Pa/s)	Density (kg/m^3)
3DPC	2316.0	698.2	27.7	1232.5	1.3126	0.312	2010
RBA-3DPC	1214.3	881.0	10.0	470.2	0.7233	0.343	1787
PCM-3DPC	3050.7	2152.9	194.8	848.6	1.0580	0.573	2049

	Print parameter	Buildability test result		
	Building rate (Pa/s)	Predicted buildable layer	Actual buildable layer	Error %
3DPC	3.96	21	27	+28.6%
RBA-3DPC	3.52	25	32	+28.0%
PCM-3DPC	4.04	56	74	+32.1%

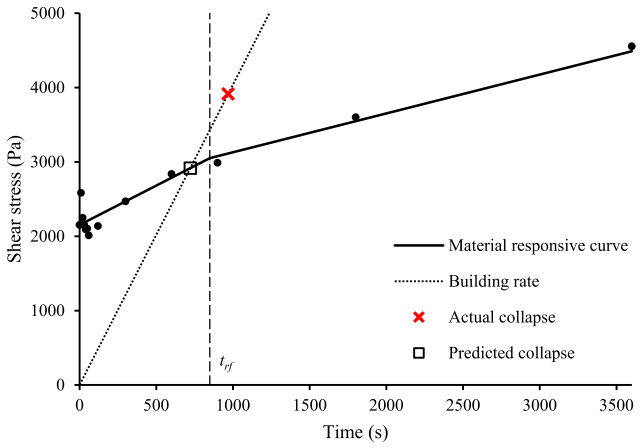

Figure 8. Buildability model of PCM-3DPC mix as an example.

the steel T-sections are schematised in Figure 5a and b. An MTS Criterion Model 40 Material Testing Machine was used to perform the DTTs on the twelve specimens, with a data acquisition rate of 10 Hz and a test rate of 0.25 mm/min.

For the UCTs, six specimens were cut from the printed section in Direction 1 and another six specimens were cut from the printed section in Direction 3. The D1 and D3 specimens for the UCTs are schematised in Figure 6a and b, with the planes shown along the faces that were subjected to compressive load. A Zwick 250 Universal Material Testing Machine was used to perform the UCTs with a loading rate of 1 mm/min.

4. Results and discussion

4.1. Rheological characterisation and buildability

The comparison of the initial CSR test responsive curve is depicted in Figure 7, showing initial static and dynamic yield stresses. It is worthwhile to highlight that the initial dynamic yield stress represents the yield capacity of freshly extruded filament. The complete data set of physical and rheological assessment, density, building rate and buildability test results are presented in Table 5.

Kruger et al. [27] addressed a simplified shear-normal stress relation applicable to 3D printed filament by introducing the strength correction factor, denoted by F_{AR}, varied by the aspect ratio of the cross-section of the extruded filament, namely $\tau = \sigma/(2 \bullet F_{AR})$. The normal stress consists of self-weight induced gravitational loading, i.e. $\sigma = \rho_{wet} \bullet g \bullet h$, where ρ_{wet} is the material wet density, g is the gravitational acceleration, and h is the filament's height. For the layer height (h) of 10 mm and layer width (w) of 45 mm giving an aspect ratio of 0.22, the strength correction factor (F_{AR}) can be obtained as 1.9 from the literature. Given the average density presented in Table 5, the approximate initial imposed shear stress by self-weight is 51.9 Pa, 46.1 Pa and 52.9 Pa for 3DPC, RBA-3DPC, and PCM-3DPC, respectively. Since all initial dynamic yield stress values are sufficiently higher, no initial plastic deformation is expected, i.e. a sound shape retention. The static yield stresses presented in Table 5 suggest good buildability, with the initial static yield stresses for all three mixes exceeding the recommended minimum [28, 29].

The stepwise loading from the successive depositions is linearised to yield a building rate by the user-defined printing parameters, e.g. print path length, print speed, filament aspect ratio. The buildability model

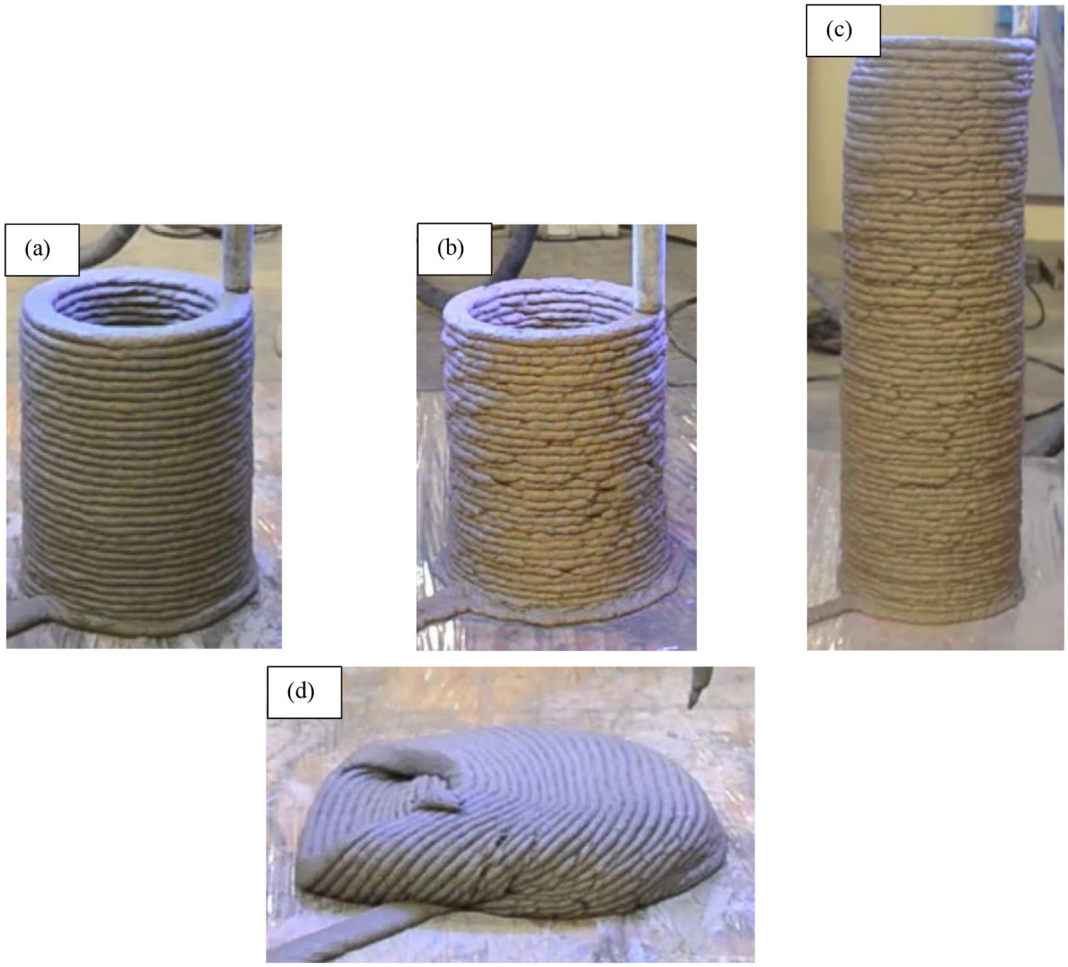

Figure 9. Print-to-collapse test results; (a) 3DPC, (b) RBA-3DPC, (c) PCM-3DPC and (d) a typical collapse subsequent to lower layer yield.

Figure 10. PCM-3DPC facade section used in thermal tests.

Table 6. Compressive cube strength and density of PCM-3DPC mix.

	Compressive Strength (MPa)	Density (kg/m^3)
Cube 1	52.5	2061
Cube 2	48.6	2056
Cube 3	49.6	2045
Cube 4	54.4	2068
Cube 5	50.0	2052
Cube 6	49.6	2035
Cube 7	49.2	2041
Cube 8	50.6	2031
Average	**50.6**	**2049**

Table 7. Comparison of compressive cube strengths and densities of RBA-3DPC, 3DPC and PCM-3DPC mixes (Coefficient of variation given in brackets).

	Compressive strength (MPa)	Density (kg/m^3)
3DPC Mix	53.1 (6.7%)	2010 (0.6%)
RBA-3DPC Mix	39.9 (3.8%)	1787 (0.5%)
PCM-3DPC Mix	50.6 (3.8%)	2049 (0.6%)

Table 8. DTT results for PCM-3DPC mix.

	D1 – intralayer (MPa)	D3 – interlayer (MPa)
Specimen 1	2.19	1.58
Specimen 2	1.88	1.35
Specimen 3	1.96	1.36
Specimen 4	1.98	1.43
Specimen 5	2.14	1.46
Specimen 6	-	1.56
Average	**2.03**	**1.46**
COV (%)	**6.5**	**6.7**

predicts the collapsing layer when the building rate curve coincides with the material responsive curve as illustrated in Figure 8. The R_{thix} values of all mixes are notably below those of the reference literature [8], 4–7 Pa/s, and this leads to all mixes failing before the re-flocculation time is reached, meaning that A_{thix} does not play a role in the failure prediction.

As per the RBA and sand grading in Figure 3, the aggregate grading of PCM-3DPC is best matched with ideal Fuller-Thompson theory. This implies a better rheological performance of material under a flow

Table 9. Comparison of DTT Results for 3DPC, RBA-3DPC and PCM-3DPC Mixes (Coefficient of variation given in brackets).

	D1 (MPa)	D3 (MPa)
3DPC Mix	-	1.72 (15.0%)
RBA-3DPC Mix	2.58 (4.7%)	1.37 (12.5%)
PCM-3DPC Mix	2.03 (6.5%)	1.46 (6.7%)

condition due to better packing density [30]. This is likely the main reason for the highest initial static yield stress and plastic viscosity of PCM-3DPC which led to the best buildability result. On the other hand, the buildability of RBA-3DPC showed a marginally better performance than 3DPC despite the lowest yield stress and viscosity which are mainly influenced by the additional water content (see Table 4). The lower gravitational loading from the subsequent printing layers due to the lower matrix density may be the primary cause of such result.

Figure 9a–d illustrates the print-to-collapse test showing the hollow columns just before collapse and a typical collapse subsequent to lower layer yield. The high dynamic yield stress of PCM-3DPC resulted in a rough surface finish since its pumpability is not favourable, however, 3DPC, with the lowest dynamic yield stress, has the finest surface finish. This aspect is not only for aesthetic purpose, but also for better interlayer bond where less surface moisture leads to weaker interlayer bond [31].

From the actual printing test, all mixes successfully printed more than the prediction model, and reached approximately ±30% offset. This agrees with a structural design parameter study performed by the same author group of the buildability model [27], where a high variation (up to 30%) was obtained during rheological characterisation process of the same constituents, but different mix batches. Shear-rate dependency of the rheological behaviour of fresh concrete also contributes to the high variation. For instance, the applied shear rated caused by the pulsation of progressive cavity pump is not identical to the controlled shear rate of the rheometer. The print quality of the PCM-3DPC mix design achieved in the print of a façade section for thermal tests is shown in Figure 10.

4.2. Compressive cube strengths

While performing compressive cube strength tests, it was observed that the average 28-day compressive strength seemed to be dependent on density which in turn seemed to be dependent on the mixing time and method. Care was therefore taken to standardise the mixing intensity, for accurate compressive cube strength and density measurements. The results of PCM-3DPC 28-day compressive cube strength tests, along with

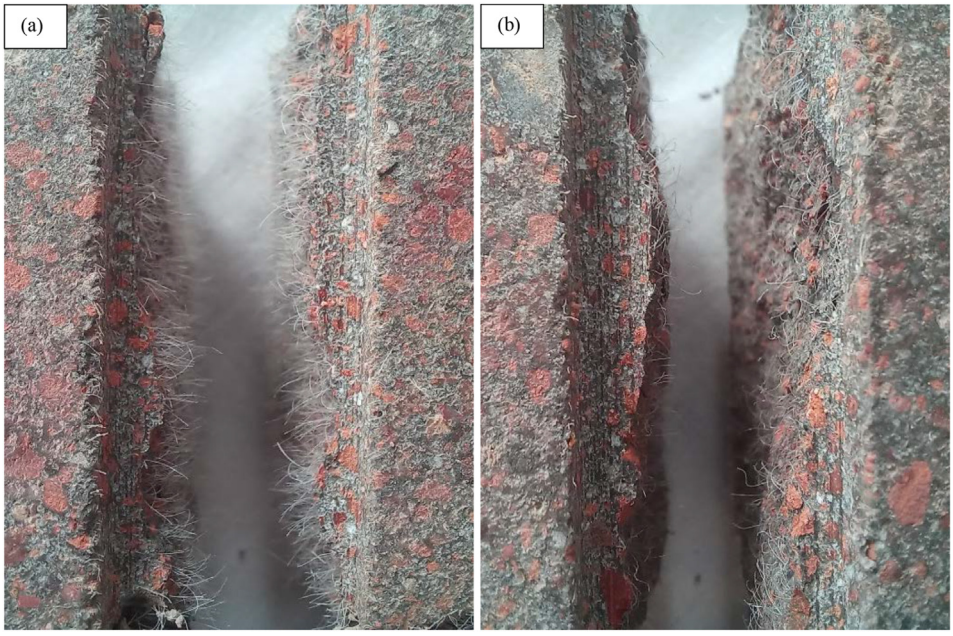

Figure 11. PCM-3DPC fractured specimens from DTT (a) D1 - intralayer (b) D3 - interlayer.

Table 10. UCT results for PCM-3DPC Mix.

	D1 – intralayer (MPa)	D3 – interlayer (MPa)
Specimen 1	32.11	32.49
Specimen 2	37.72	32.23
Specimen 3	27.19	31.23
Specimen 4	32.05	29.08
Specimen 5	35.26	28.26
Specimen 6	39.62	37.28
Average	**33.99**	**31.76**
COV (%)	13.2	10.1

Table 11. Comparison of UCT Results for 3DPC, RBA-3DPC and PCM-3DPC Mixes (Coefficient of variation given in brackets).

	D1 (MPa)	D3 (MPa)
3DPC Mix	27.75 (7.8%)	36.52 (8.0%)
RBA-3DPC Mix	23.75 (11.9%)	29.06 (11.4%)
PCM-3DPC Mix	33.99 (13.2%)	31.76 (10.1%)

the density are listed in Table 6, and the comparison of these results with the results of the two other mixes is shown in Table 7. The RBA-3DPC mix has both the lowest density and lowest compressive cube strength, while the densities and compressive cube strengths of the 3DPC and PCM-3DPC mixes are similar. The high density achieved in the PCM-3DPC mix gives an indication that the technique of vacuum impregnation was successful in adding the PCM to the pores of the RBA, creating a denser TESA.

4.3. Tensile 3DPC strengths

The results of the PCM-3DPC DTTs are listed in Table 8 and the comparison of these results with the two other mixes is shown in Table 9. There were only five valid results for PCM-3DPC D1 because during testing one specimen broke at its joint to the steel T-section due to insufficient gluing. The average interlayer tensile strength of the PCM-3DPC was 6% higher than that of the RBA-3DPC and 15% lower than that of the 3DPC.

The ratio of interlayer to intralayer tensile strength of the PCM-3DPC specimens was 0.72. The reduced strength in the interlayer direction is due to the lack of fusion (LOF) between the layers, as reported by Kruger and van Zijl [32], although the difference is not as significant as for the RBA-3DPC specimens, for which an interlayer to intralayer tensile strength ratio of 0.53 was reported by Christen et al. [1]. D1 and D3 PCM-3DPC specimens after fracture are shown in Figure 11a and b. The fibres are visible in both specimens but even more so in the intralayer specimen, in which they can be seen aligned in the direction of the layer.

4.4. Compressive 3DPC strengths

The results of the PCM-3DPC UCTs are listed in Table 10 and the comparison of these results with the two other mixes is shown in Table 11. The average D1 compressive strength of the PCM-3DPC was 22% higher than that of the 3DPC and 43% higher than that of the RBA-3DPC. The average D3 compressive strength of the PCM-3DPC was 13% lower than that of the 3DPC and 9% higher than that of the RBA-3DPC.

The ratio of compressive strength of Direction 1 to Direction 3 for PCM-3DPC was 1.07. It is interesting to note that the stronger direction recorded for the PCM-3DPC was opposite to that recorded for the RBA-3DPC and 3DPC, where the ratio of compressive strength of D1 to D3 was 0.82 and 0.76 respectively. 3DPC, RBA-3DPC and PCM-3DPC specimens from the UCTs are shown in Figure 12a–f.

4.5. PCM leakage investigation

While working with the PCM-3DPC cast cubes, it was observed that when taken out of the climate-controlled room and exposed to higher temperatures, the colour of the cubes darkened over several hours, as shown in Figure 13. It was hypothesised that this could be due to some PCM leaking from the pores of the RBA and making its way to the surface of the concrete. Several researchers have investigated techniques of coating TESAs to prevent PCM leakage. Sani et al. [33] applied two coatings of primer epoxy resin and graphite powder to PCM impregnated lightweight aggregates while Hassan et al. [6] coated PCM impregnated lightweight expanded clay aggregate with geopolymer paste.

In the current study, no coating techniques have been adopted therefore it is important to understand and quantify PCM leakage - firstly leakage out of the RBA pores and into the concrete matrix, as this could

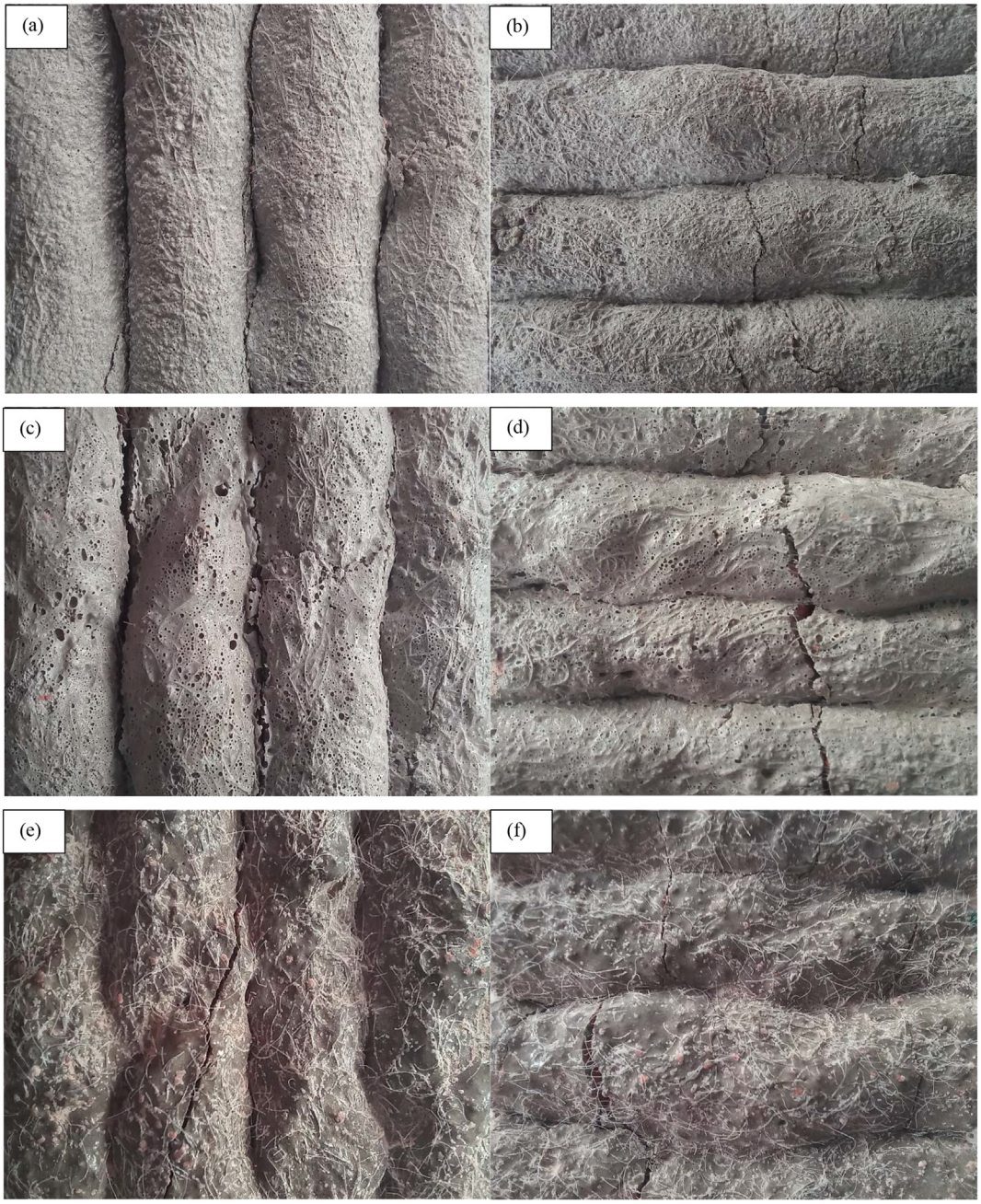

Figure 12. Specimens after UCTs (a) 3DPC D1 (b) 3DPC D3 (c) RBA-3DPC D1 (d) RBA-3DPC D3 (e) PCM-3DPC D1 (f) PCM-3DPC D3.

have an effect on long-term concrete strength, and secondly leakage out of the concrete, as this could have an effect on long-term PCM effectiveness. No leakage was observed during mixing and printing, after visual scrutiny for PCM residue in the mixer, pump and printer, but internal and external leakage subsequent to mixing and printing should still be considered. To ascertain whether PCM leaked out of the pores of the RBA, SEM imaging in conjunction with energy-dispersive X-ray spectroscopy (EDX/EDS) was used to visualise the PCM in samples that were cut from printed specimens of PCM-3DPC at an age of roughly seven months. To quantify effects of any leakage into the concrete matrix on mechanical strength, 90-day compressive strength tests were performed on cubes cast from PCM-3DPC. Mass-loss tests on PCM-3DPC cubes placed in the oven at 50 °C for seven days were used to determine whether PCM leaked out of the concrete, which would affect the total latent heat capacity of the concrete mix over time.

4.5.1. Scanning electron microscopy analysis

To initiate the SEM analysis, for a reference of scale and texture, the surface of 2 mm RBA particles were first analysed with SEM imaging, as shown in Figure 14a at 100× magnification, before analysing the PCM-3DPC specimens. Organic paraffin is made up of carbon and hydrogen and hydrogen is unable to be detected by EDX analysis, therefore peaks of carbon were used to indicate the presence of PCM in the PCM-3DPC samples, which presented as darker shades of grey with SEM imaging. Figure 14b shows concentrations of PCM in the exposed pores of an RBA particle which is partly obscured by the concrete matrix.

The RBA samples areas and the PCM-3DPC sample areas for EDX spectrums are shown in Figure 15a and b and Figure 16. The RBA and PCM-3DPC sample areas for the EDX map sum spectrum are shown in Figures 17 and 18 respectively, and are the same areas as those shown in the SEM images of Figure 14.

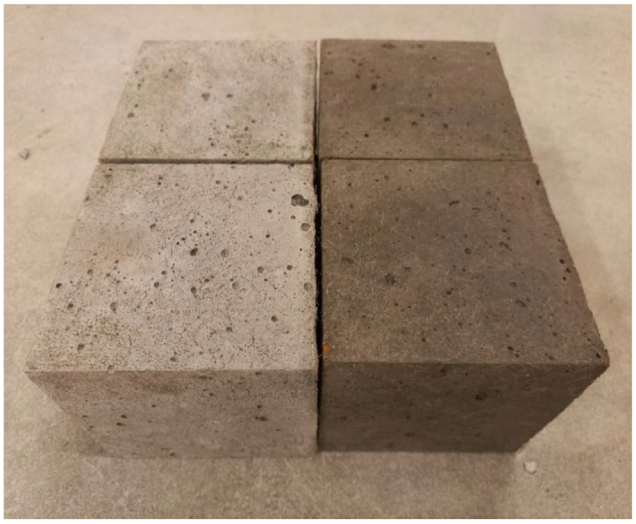

Figure 13. Colour change of PCM-3DPC cubes.

The EDX results for all RBA spectrums are shown in Figure 19 and for all PCM-3DPC spectrums are shown in Figure 20. No matter the sample area, the elements present in the RBA are relatively uniformly concentrated, however the spectrums of the PCM-3DPC vary depending on the constituent of concrete that dominates in a particular sample area, which is more clearly shown by the element mapping of PCM-3DPC in Figure 18. From Figure 18 it can be seen, pointed out with arrows, that the turquoise concentrations indicating carbon (PCM) are superimposed on the yellow concentrations indicating silicon (which is richly present in RBA) and separate from the pink concentrations indicating calcium (present in the cement of the concrete matrix). The yellow concentrations without turquoise concentrations (towards the bottom left of Figure 18) are believed to indicate the silicon present in the natural aggregate. Although it is clear that the PCM remains concentrated around the pores of RBA, it cannot be ruled out that some PCM does leak out of the RBA pores into the concrete matrix - PCM-3DPC EDX Spectrum 2 shows a 20.4% weight percentage of carbon in the concrete matrix.

4.5.2. *Effect on strength*

90-day cube strength tests were performed on four PCM-3DPC cubes to determine long term effects of any internal leakage of PCM on mechanical strength. Cube 1 and Cube 2 were placed in an oven at 50 °C for seven days of the 90-day period in an attempt to accelerate any PCM leakage from the pores of RBA, and Cube 3 and Cube 4 remained in the climate-controlled room (at a temperature of 22 ± 2 °C and relative humidity of 65 ± 5%) for the entire 90-day period up until strength testing. The 90-day strengths were compared to the average 28-day strength, as well as the 90-day strength prediction (which was calculated as 1.14 times the 28-day strength). The results of these strength tests are shown in Table 12. Although the 90-day cube strengths of the

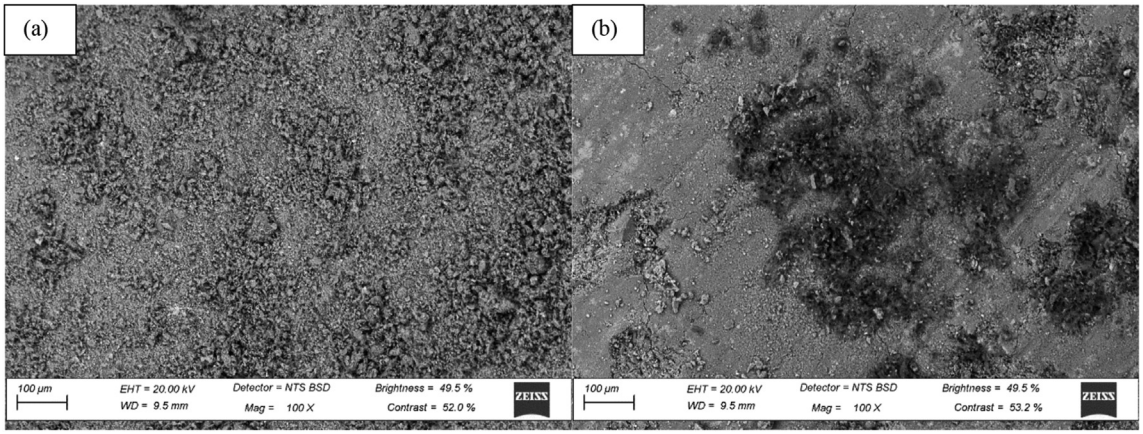

Figure 14. At 100x magnification (a) 2 mm RBA particle (b) saw cut surface of PCM-3DPC specimen.

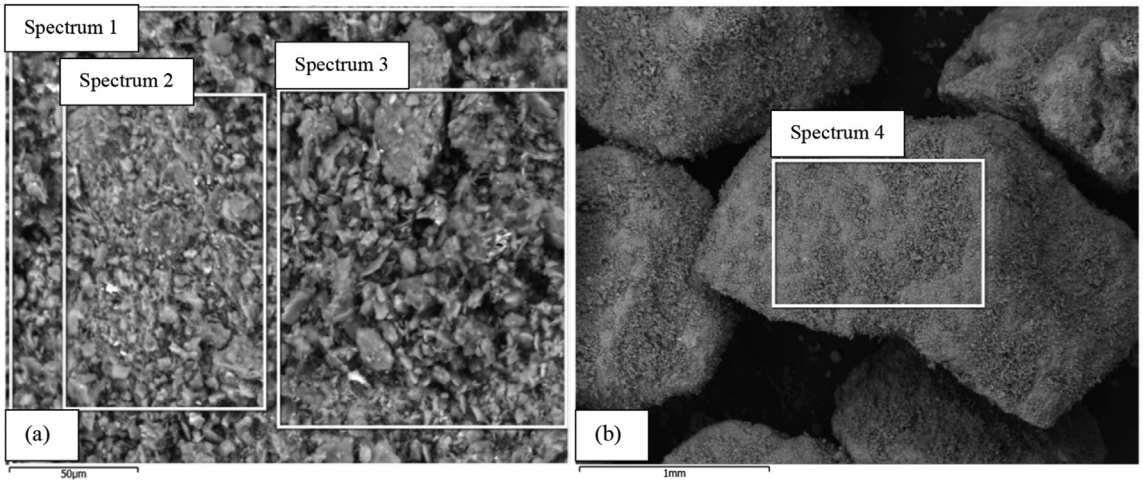

Figure 15. Sample areas for RBA EDX spectrums.

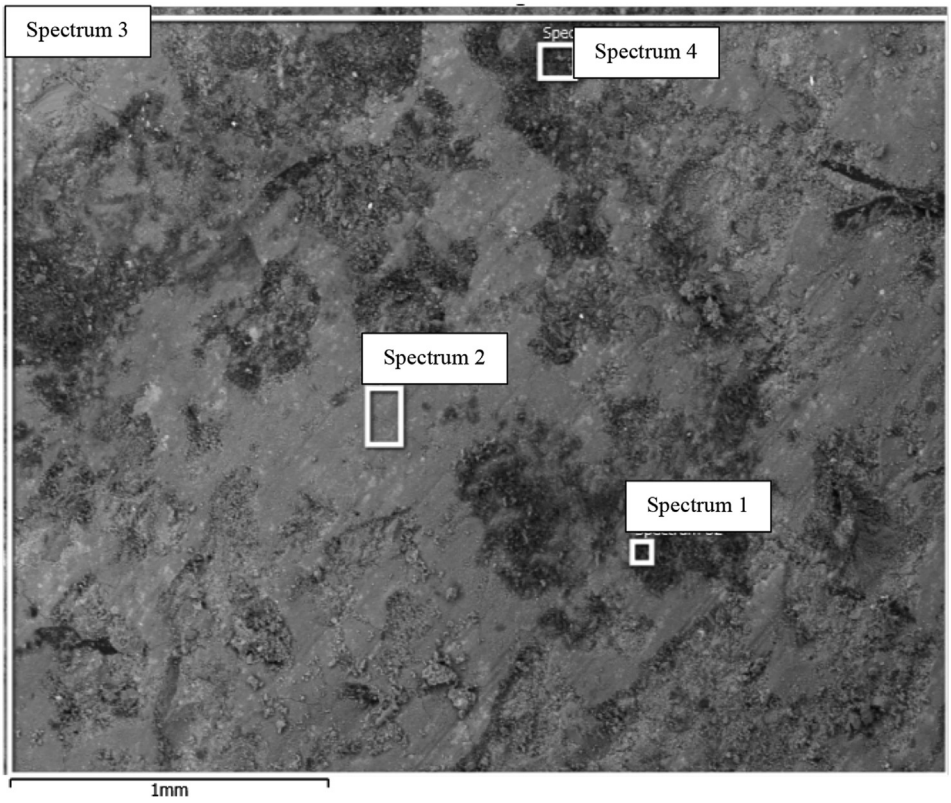

Figure 16. Sample areas for PCM-3DPC EDX spectrums.

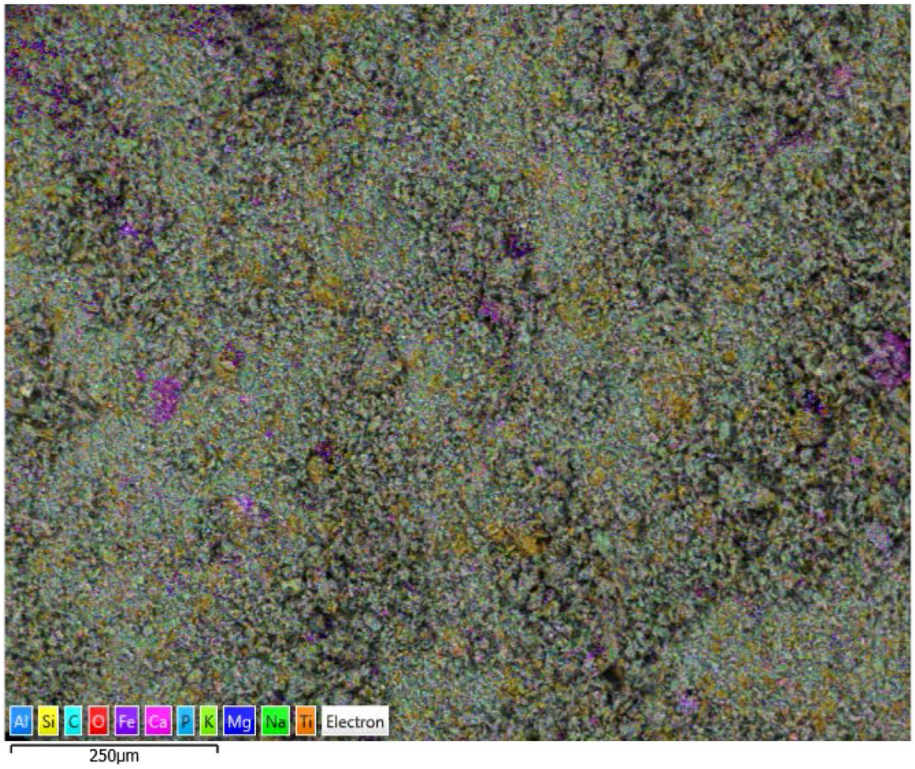

Figure 17. RBA map sum spectrum area.

two cubes that were placed in the oven for 7 days are slightly lower, all 90-day cube strengths exceeded the 28-day cube strength, with an average only 3% lower than the 90-day strength prediction. It is worth noting that the strengths reported in Table 12 are lower than those reported in Table 6 for PCM-3DPC because of the difference in mixing method as discussed in Section 4.2. The mix reported in Table 12 had not been vibrated in the hopper of the 3DPC pump and lower densities and compressive strength were recorded as a result.

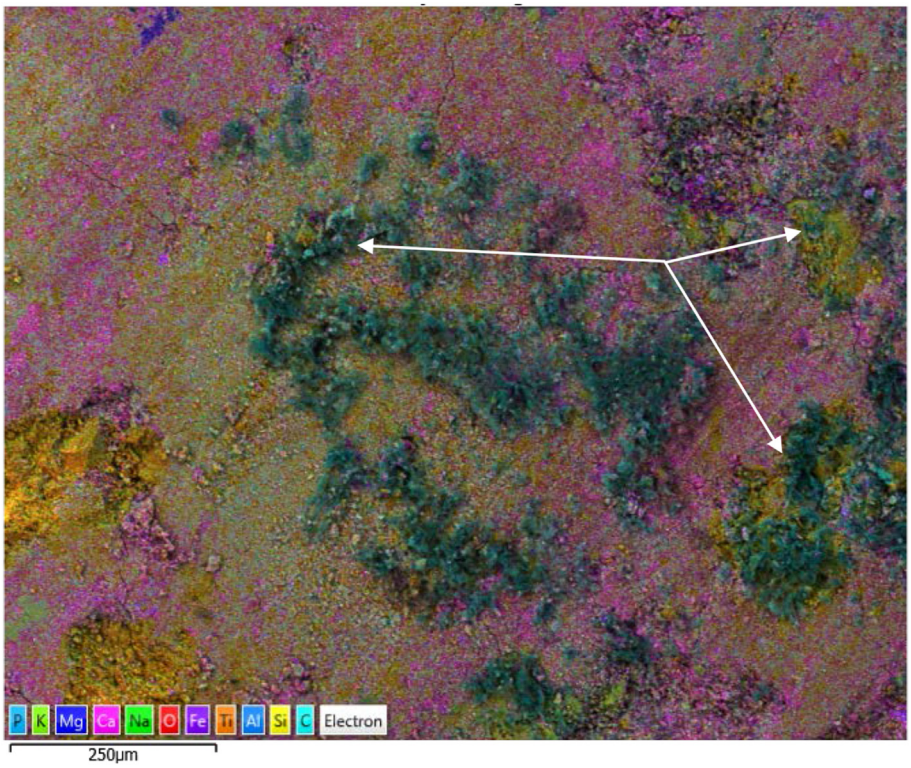

Figure 18. PCM-3DPC map sum spectrum area.

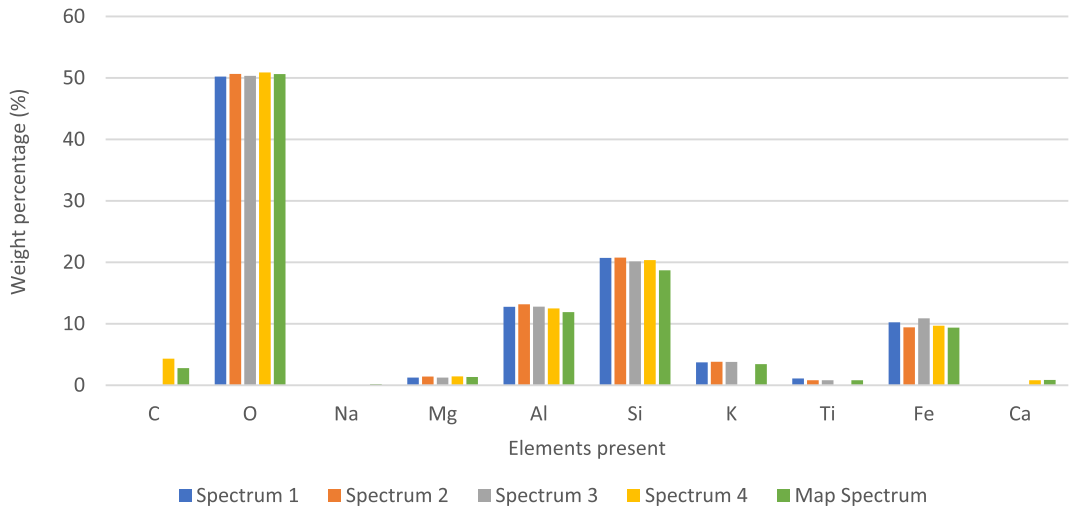

Figure 19. EDX results for RBA.

4.5.3. Mass-loss tests

Mass-loss tests were performed to determine whether PCM leaked out of the concrete when exposed to temperatures above the melting temperature of the PCM. For these tests two PCM-3DPC cubes and two RBA-3DPC cubes were taken from the climate-controlled room after their 28-day curing period and placed in an oven at 50 °C for seven days while another two PCM-3DPC cubes and two RBA-3DPC cubes were left in the climate-controlled room for the same time. The RBA-3DPC cubes were used as a control, to ascertain how much of the mass loss could be attributed to water evaporation. The mass lost in each cube as a percentage of the original mass is shown in Table 13.

From Table 13 it is clear that the mass loss in the RBA-3DPC cubes was in fact greater than the mass loss in the PCM-3DPC cubes. It is assumed that mass loss is probably entirely due to evaporation of water and not leakage of PCM out of the concrete at temperatures up to 50 °C. The RBA-3DPC mix had a higher w/c ratio (0.57 compared to 0.45), which would explain a higher rate of water evaporation from the concrete.

Subsequent to SEM imaging, 90-day strength tests and mass-loss tests, the authors maintain that the effect of leakage can be considered negligible.

4.6. Discussion

Assessing all of the mechanical characterisation results together, it is evident that the PCM-3DPC has improved strengths compared to the RBA-3DPC. This is likely due to the increased density of the TESA compared to the RBA, as it is known that the strength of concrete decreases with increasing porosity [34]. The anomalies in the results are that: i) the PCM-3DPC D1 tensile 3DPC strength is surprisingly low, and is

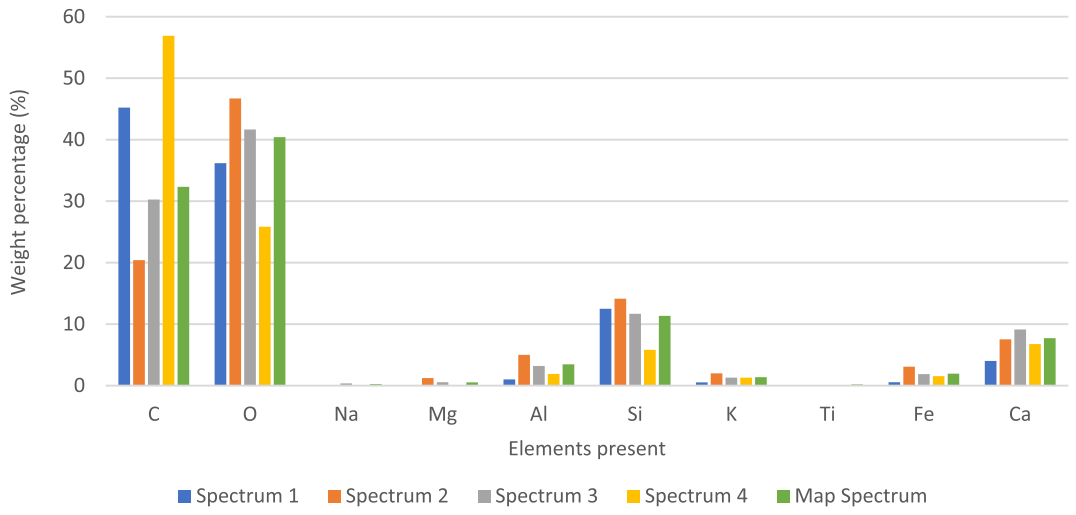

Figure 20. EDX results for PCM-3DPC.

Table 12. 28-day and 90-day compressive cube strengths of PCM-3DPC mix (Coefficient of variation given in brackets).

	28-day Compressive Strength (MPa)
28-day average	40.0 (1.0%)
90-day prediction	45.6
	90-day Compressive Strength (MPa)
Cube 1	43.0
Cube 2	42.8
Cube 3	45.6
Cube 4	45.0
Average	**44.1 (3.2%)**

the only strength result lower than the corresponding result for RBA-3DPC and ii) the dominant compressive 3DPC strength direction for the PCM-3DPC was opposite to the dominant direction recorded for RBA-3DPC and 3DPC.

The reasons for these anomalies are not fully understood but hypotheses can be formed based on current knowledge of the concepts of LOF, heat of hydration, particle and water migration in concrete, and most importantly, the effect of PCM on all of these concepts.

LOF is a well-known concept in the field of additive manufacturing and refers to the weaker interlayer region of printed elements. Research by Kruger and van Zijl [32] discusses mechanisms responsible for LOF, namely loss of surface moisture, air entrapment, thixotropy and surface roughness. Loss of surface moisture was reported as the main mechanism responsible for LOF. Immediately after extrusion of concrete, water evaporates from the surface at a rate which is dependent on the surrounding temperature, relative humidity and wind speed. The surface of the concrete becomes drier, and when a new layer of concrete is deposited on top, water migrates from the fresh top layer to the drier layer below. At the same time, air is pushed up to the interlayer region and the top layer. The increased air content in the interlayer region leads to an increase in porosity and poorer bond quality, or LOF. Kruger and van Zijl [32] also discussed how increased surface roughness leads to improved bond strength between deposited layers and lower LOF.

Table 13. Percentage mass lost in PCM-3DPC and RBA-3DPC cubes.

	% Mass Lost In Oven		% Mass Lost In Climate-Controlled Room	
	Cube 1	Cube 2	Cube 3	Cube 4
PCM-3DPC	1.34	1.33	≈ 0	≈ 0
RBA-3DPC	2.02	1.93	≈ 0	≈ 0

De Schutter and Taerwe [35] measured the heat of hydration of hardening concrete by isothermal tests at 5, 20 and 35 °C. Their 20 °C isothermal test results for the heat production rate of Portland cement CEM I 52.5 with a water to cement ratio of 0.5 can be interpreted to give an adiabatic temperature evolution curve of hardening concrete using the second law of thermodynamics [36], as shown in Eq. (5):

$$\delta T = \frac{\delta Q \cdot m_c}{\rho \cdot C_p} \tag{5}$$

where δT (°C) is the increase in temperature caused by an increase in heat production δQ (J/kg), m_c is the mass of cement per cubic meter of concrete (kg/m^3), ρ is the density of the concrete (kg/m^3) and C_p is the specific heat capacity of the concrete (J/kg°C).

For the calculation, the value of m_c was taken as 521 kg/m^3, ρ was taken as 2049 kg/m^3, and C_p was assumed to be 900 J/kg°C. The heat production rate of Portland cement CEM I 52.5 measured by De Schutter and Taerwe [35] is shown in Figure 21 alongside the temperature evolution curve calculated using Eq. (5). From the temperature evolution curve, it can be seen that the temperature of hardening concrete may reach temperatures above 90 °C in the first 120 h, if perfectly insulated and no heat is lost to the surroundings.

In research by Šavija and Schlangen [36] it was concluded that the addition of PCM to hardening concrete delays the temperature rise, and lowers the maximum stresses experienced in the concrete, potentially mitigating early age thermal cracking. It is possible that the PCM used in this current research positively affected the strength of the concrete by the same mechanism, as well as by slowing water evaporation in the printed concrete, resulting in less severe lack of fusion. This could help to explain the abnormally high D1 PCM-3DPC compressive strength, as the lower D1 compressive strength of the RBA-3DPC and 3DPC had been attributed to lack of fusion leading to delamination and reduced confinement [1].

The same explanation cannot be used for the abnormally low intralayer tensile strength of the PCM-3DPC. When comparing samples of the three mixes, it was noticed that the outside of the PCM-3DPC appeared considerably more fibrous, even though the three mixes contained exactly the same amounts of fibre (as stated in Table 4). This can be seen in Figure 12. It is hypothesised that the PCM addition to the mix, and increased viscosity of the PCM-3DPC mix affects the particle migration in the mix, causing the fibres to separate and move to the outside of the extruded layer, although the mechanism by which this occurs is not fully understood. For the RBA-3DPC and 3DPC printed specimens, it had been observed that the fibres aligned themselves along the direction of layer extrusion, contributing somewhat to an increased intralayer tensile strength. An uneven distribution of the fibres due to their migration to

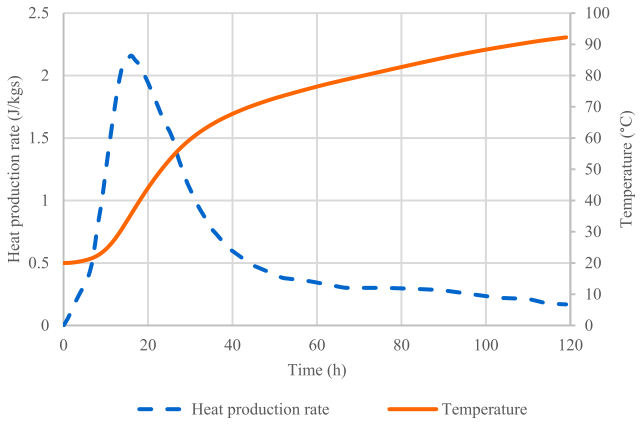

Figure 21. Heat production rate and adiabatic temperature of hardening concrete.

the outside of the extruded layer may be the cause of the lower PCM-3DPC intralayer tensile strength.

5. Conclusions

In this research paper, the potential for sustainable buildings through recycling and internal climate control with PCM infused RBA was addressed. The addition of PCM to RBA-3DPC, and the resulting effects on its strength and printability were studied. The following conclusions can be drawn:

- Successful incorporation of and mix design with PCM in 3DPC by vacuum impregnation of RBA was demonstrated. The mix design contained 75 kg PCM per m^3 of concrete.
- The rheology indicates that buildability of PCM-3DPC is favourable as it had the highest yield stress of the mixes considered and comparable R_{thix} value, resulting in the highest number of buildable layers predicted and realised.
- Compressive cube strengths exhibit dependence on density, and hence mixing time and method. The high density and compressive cube strength of PCM-3DPC relative to RBA-3DPC are indicative of successful vacuum impregnation technique.
- Overall, in the 3DP format, PCM-3DPC exhibits greater strength relative to RBA-3DPC, and lower strength compared to 3DPC. The PCM-3DPC exceeds the RBA-3DPC interlayer (D3) tensile strength by 6%, the intralayer (D1) compressive strength by 43% and the interlayer (D3) compressive strength by 9%. The PCM-3DPC subceeds the 3DPC interlayer (D3) tensile strength by 15% and the interlayer (D3) compressive strength by 13%.
- Notable exceptions to the strength findings are the lower PCM-3DPC intralayer (D1) tensile strength (possibly due to fibre migration to outer edges during the extrusion process) and the dominant PCM-3DPC compressive strength direction (D1) being converse to both RBA-3DPC and 3DPC mixes (potentially due to the positive effect PCM has in delaying the temperature rise during hardening and subsequent reduced stresses and early age cracking).
- There was no leakage of PCM out of the PCM-3DPC detected when continuously exposed to temperatures of up to 50 °C and no negative effects of any internal leakage on long term (90-day) compressive strength.

Declarations

Author contribution statement

Heidi Christen & Seung Choa: Conceived and designed the experiments; Performed the experiments; Analyzed and interpreted the data; Wrote the paper.

Gideon van Zijl & Wibke de Villiers: Conceived and designed the experiments; Analyzed and interpreted the data; Contributed reagents, materials, analysis tools or data.

Funding statement

This research did not receive any specific grant from funding agencies in the public, commercial, or not-for-profit sectors.

Data availability statement

Data will be made available on request.

Declaration of interest's statement

The authors declare no conflict of interest.

Additional information

No additional information is available for this paper.

References

[1] H. Christen, G. van Zijl, W. de Villiers, The incorporation of recycled brick aggregate in 3D printed concrete, Clean. Mater. 4 (2022) 100090.
[2] M. Jarraud, A. Steiner, Climate Change 2014 Synthesis Report vol. 9781107025, 2015.
[3] A. Zhou, K.W. Wong, D. Lau, Thermal insulating concrete wall panel design for sustainable built environment, Sci. World J. 2014 (2014).
[4] L.F. Cabeza, C. Castellón, M. Nogués, M. Medrano, R. Leppers, O. Zubillaga, Use of microencapsulated PCM in concrete walls for energy savings, Energy Build. 39 (2) (2007) 113–119.
[5] A.A.A. Gassar, G.Y. Yun, Energy saving potential of PCMs in buildings under future climate conditions, Appl. Sci. 7 (12) (2017).
[6] A. Hassan, A.H.I. Mourad, Y. Rashid, N. Ismail, M.S. Laghari, Thermal and structural performance of geopolymer concrete containing phase change material encapsulated in expanded clay, Energy Build. 191 (2019) 72–81.
[7] C. Mankel, A. Caggiano, E. Koenders, Thermal energy storage characterization of cementitious composites made with recycled brick aggregates containing PCM, Energy Build. 202 (2019), 109395.
[8] J. Kruger, S. Zeranka, G. van Zijl, 3D concrete printing: a lower bound analytical model for buildability performance quantification, Autom. ConStruct. 106 (2019).
[9] A. Caggiano, C. Mankel, E.A.B. Koenders, Reviewing Theoretical and Numerical Models for PCM-Embedded Cementitious Composites, 2019.
[10] M. Pomianowski, P. Heiselberg, R.L. Jensen, R. Cheng, Y. Zhang, A new experimental method to determine specific heat capacity of inhomogeneous concrete material with incorporated microencapsulated-PCM, Cement Concr. Res. (2014).
[11] K. Pielichowska, K. Pielichowski, Phase change materials for thermal energy storage, Prog. Mater. Sci. (2014).
[12] A. Sharma, V.V. Tyagi, C.R. Chen, D. Buddhi, Review on thermal energy storage with phase change materials and applications, Renew. Sustain. Energy Rev. (2007).
[13] D.P. Bentz, R. Turpin, Potential applications of phase change materials in concrete technology, Cem. Concr. Compos. 29 (7) (Aug. 2007) 527–532.
[14] T.C. Ling, C.S. Poon, Use of phase change materials for thermal energy storage in concrete: an overview, Construct. Build. Mater. 46 (2013) 55–62.
[15] D. Zhang, Z. Li, J. Zhou, K. Wu, Development of thermal energy storage concrete, Cement Concr. Res. 34 (6) (2004) 927–934.
[16] A. Hassan, N. Ismail, A.H.I. Mourad, Y. Rashid, M.S. Laghari, Preparation and characterization of expanded clay-paraffin wax-geo-polymer composite material, Materials 11 (11) (2018).
[17] D. Ormandy, V. Ezratty, Health and thermal comfort: from WHO guidance to housing strategies, Energy Pol. 49 (2012) 116–121.
[18] Southern African Universities Radiometric Network. https://sauran.ac.za/, 2021.
[19] Rubitherm Technologies GmbH, "Technical data sheet RT25HC," Tech. Data sheet RT25HC, p. 1 [Online]. Available: https://www.rubitherm.eu/media/products/datasheets/Techdata_-RT25HC_EN_15012020.PDF, 2020.
[20] SANS3001-AG21, SANS 3001-AG21: 2014 SOUTH AFRICAN NATIONAL STANDARD Civil Engineering Test Methods Part AG21 : Determination of the Bulk Density , Apparent Density and Water Absorption of Aggregate Particles Passing the 5 Mm Sieve for Road Construction Materials, 2014.
[21] S. Cho, J. Kruger, F. Bester, M. van den Heever, A. van Rooyen, G. van Zijl, A compendious rheo-mechanical test for printability assessment of 3D printable concrete cement, in: 2nd RILEM Int. Conf. Concr. Digit. Fabr. 3, 2020, pp. 1–10.
[22] Germann Instruments, ICAR Plus Rheometer. http://germann.org/products-by-application/rheology-of-concrete/icar-rheometer (accessed Jun. 15, 2020).
[23] J. Kruger, S. Zeranka, G. van Zijl, An ab initio approach for thixotropy characterisation of (nanoparticle-infused) 3D printable concrete, Construct. Build. Mater. 224 (2019) 372–386.
[24] N. Roussel, A thixotropy model for fresh fluid concretes: theory, validation and applications, Cement Concr. Res. 36 (10) (2006) 1797–1806.

[25] S. Cho, P.J. Kruger, S. Zeranka, G.P.A.G. van Zijl, 3D Printable concrete technology and mechanics, Concr. Soc. (2019) 11–18.
[26] SANS5863, SANS 5863: 2006 South African National Standard Concrete Tests — Compressive Strength of Hardened concrete, 2006, pp. 2–6.
[27] J. Kruger, S. Cho, S. Zeranka, C. Viljoen, G. Van Zijl, 3D concrete Printer Parameter Optimisation for High Rate Digital Construction Avoiding Plastic Collapse 183, 2019, 2020.
[28] T.T. Le, S.A. Austin, S. Lim, R.A. Buswell, A.G.F. Gibb, T. Thorpe, Mix design and fresh properties for high-performance printing concrete, Mater. Struct. Constr. 45 (8) (2012) 1221–1232.
[29] V. Mechtcherine, et al., Extrusion-based additive manufacturing with cement-based materials – production steps, processes, and their underlying physics: a review, Cement Concr. Res. 132 (2020), 106037.
[30] Y. Weng, M. Li, M.J. Tan, S. Qian, Design 3D printing cementitious materials via Fuller Thompson theory and Marson-Percy model, Construct. Build. Mater. 163 (2018) 600–610.
[31] G.M. Moelich, J. Kruger, R. Combrinck, Modelling the interlayer bond strength of 3D printed concrete with surface moisture, Cement Concr. Res. 150 (September) (2021), 106559.
[32] J. Kruger, G. van Zijl, A compendious review on lack-of-fusion in digital concrete fabrication, Addit. Manuf. 37 (2021), 101654.
[33] A.K. Sani, I.O. Olawoore, R.M. Singh, Assessment of impregnating phase change materials into lightweight aggregates for development of thermal energy storage aggregate composites, Construct. Build. Mater. 305 (2021), 124683.
[34] C. Lian, Y. Zhuge, S. Beecham, The relationship between porosity and strength for porous concrete, Construct. Build. Mater. 25 (11) (2011) 4294–4298.
[35] G. De Schutter, L. Taerwe, General hydration model for portland cement and blast furnace slag cement 25, 1995, pp. 593–604, no. 3.
[36] B. Šavija, E. Schlangen, Use of phase change materials (PCMs) to mitigate early age thermal cracking in concrete: Theoretical considerations, Construct. Build. Mater. 126 (2016) 332–344.